International Journal of Concrete Structures and Materials
Vol.18, No.1E, pp.35~41, June 2006

A Mechanical Model of the End Anchorage Zone of Prestressed Concrete Members

Won-Ho Kang,[1] Young-Min You,[2] Seung-Hyun Oh,[3] and Sang-Woo Lee[4]

(Originally published in Korean version of *Journal of KCI*, Vol.8, No.4, July 1996)

Abstract: It is expected that recent development of mechanical models will soon supersede previous empirical methods of detailing. In this study, a mechanical model is proposed to analyze the behavior of the anchorage zone of prestressed concrete members. The main characteristics of the proposed model lies in its rational consideration of material properties such as concrete strength in biaxial stress state and that of local zone reinforced by spirals. The shear friction strength of concrete surrounding a spiral is also considered. The computational results of the proposed model as well as the existing Strut-and-Tie model (STM) and nonlinear finite element analysis are compared with experimental results. The results of the comparison revealed that the proposed model showed better prediction of the failure mode as well as the failure load. Additionally, the proposed model also explained the three-dimensional failure mechanism very well, while other methods based on two-dimensional analysis could not do so well.

Keywords: mechanical model, anchorage zone, detailing, prestressed concrete.

1. Introduction

A problem related to the anchorage zone of prestressed concrete members can be classified as a stress state problem induced by a concentrated force, so called mechanical D-region problem.[1] Since we cannot apply the hypothesis that plan section remains plane on this local zone near the concen-trated force, it is impossible to predict the stress accurately based on the engineering beam theory. The principle of Saint-Venant governs the stress state of the local zone. Thus, we cannot apply conventional design methods.[6,7]

Conventionally we designed the local zone by empirical rules or experiments pertaining to individual local zone case by case, not by mechanically rational methods. Although practical engineers recognized that simple empirical rules of detailing cannot be applied to various cases of reinforced detailing problems,[2] it was Fritz Leonhardt[3] who let researchers know that reinforcement detailing should be determined based on the mechanical principles, the leading reseacher for active study of reinforcement detailing design. Ever since Mörsh first used a mechanical model for shear design of a member, engineers have continuously wanted to use a rational and understandable mechanical model to the plane or three-dimensional problems. Some researchers in Denmark[4] and Swiss[5] showed that it is easier to constitute a mechanical model at the ultimate state of reinforced concrete members because the force flow at the plastic state is quite simpler than the elastic state.

Their theories are known as limit analyses, which are not used in general as design rules for the reason that the lower bound solution does not guarantee the required accuracy and that the rigid plastic assumption of concrete stress-strain relationship is not easily satisfied. However, the assumption of simpler stress state for concrete members at ultimate state is a very attractive idea to design engineers, who need an intuitional tool for reinforcement detailing. Plastic properties of concrete are better understood recently, and the accuracy of the limit analysis model is much enhanced. As a consequence, some good results based on limit analysis have been reported. In this study we apply a mechanical model, which is based on the plasticity theory, to the problem of predicting the behavior of prestressed concrete members at the end anchorage zone.

2. Material properties of concrete for building a mechanical model

2.1 Concrete compressive strength under biaxial stress state

In the mechanical model, biaxial or tri-axial stress state of concrete elements is simplified as uni-axial stress state with respect to the stress distribution of plastic state. However, the strength of elements should be estimated based on real stress state of the element, regardless of the reinforcement. Compressive strength of bi-axial state was extensively studied by Ahmad, Shah,[8] and Vecchio and Collins[9] who proposed a formula for compressive strength at biaxial stress state. Their formula can be applied to typical prestresssed concrete members, while the effective strength of high-strength concrete should be reduced as reported by Muttoni[10] from the results of shear test.

[1] KCI member, Dept. of Civil Ergineering, Dong-A University, Pusan 604-714, Korea. *E-mail: whkang@dau.ac.kr*
[2] University Michigan, MI 48502, USA.
[3] Dong A University, Pusan 604-714, Korea.
[4] You-Shin Corporation Seoul 135-936, Korea.

In this study we use Vecchio and Collins formula to calculate bi-axial compressive strength of the members, of which the strength at 28 days is lower than 40 MPa. The equation is as follows.

$$\frac{f_{c2}}{f'_{ck}} = \frac{1}{0.8 + 170\varepsilon_1} \leq 1.0 \quad (1)$$

Where,

f_{c2} = compressive strength of concrete at bi-axial stress state

f_{ck}' = compressive strength of concrete at uni-axial stress state

ε_1 = strain in principal direction

When a member is reinforced in one direction, with the difference in angle between the reinforcement direction and principal stress direction, the following relationship holds for the strain of reinforcement and strain of principal direction.

$$\varepsilon_1 = \varepsilon_s + (\varepsilon_s + 0.002)\cot^2\alpha_s \quad (2)$$

Where,

ε_1 = principal strain

ε_s = reinforcement strain

α_s = angle between reinforcement and principal direction

2.2 Concrete bearing strength under an anchorage plate

The stress state of concrete under an anchorage plate depends on friction between the anchorage plate and concrete as well as the restraining effect of surrounding concrete. Bearing strength of concrete is not estimated well enough by a theoretical model, in spite that we can explain the formation of stress wedge by the plasticity theory. In this study, we adopt a formula for bearing strength, which depends on bearing area and surrounding concrete area, based on the test results of Hawkins.[12]

$$f_{bearing} = 0.85f'_c\sqrt{\frac{A_2}{A_1}} \quad (3)$$

Where,

$$\sqrt{\frac{A_2}{A_1}} \leq 2.0$$

A_1 = possible maximum area of surrounding concrete, of which the loading center gets the shape of a centroid.

A_2 = net loading area

2.3 Compressive strength of three-dimensional stress state confined by spirals

The compressive strength of a concrete cylinder, which is confined by spirals, increases by the confining degree of spirals. Transverse stress can be calculated according to the Kanellopoulos' stress model.[13]

$$\sigma_1 = -\frac{\omega_t f'_c}{1 - \frac{\pi}{4}\frac{s}{d_c}} \quad (4)$$

Where,

$$\omega_t = \frac{2 \cdot A_s \cdot f_y}{s \cdot d_s \cdot f'_c}$$

d_s = diameter of spiral

s = space of spirals

A_s = Area of spiral

f_y = yield stress of spirals

Richart[14] reports that the compressive strength of concrete at three-axial stress state increases in accordance with the transverse stress.

$$\Delta f_{c3} = -4 \cdot \sigma_1 \quad (5)$$

Thus, we can calculate the average compressive strength of core concrete as follows.

$$\frac{f_{c3}}{f'_c} = 1 + 4 \cdot \omega_t \cdot \frac{\left(1 - \frac{s}{d_s}\right)^2}{1 - \frac{\pi}{4} \cdot \frac{s}{d_s}} \quad (6)$$

Concrete ahead of the spiral end is subject to the same condition as the concrete under anchor plate. Compressive strength of core concrete in the spiral can be calculated by Eq. (6), while compressive strength of concrete ahead of the spiral end can be calculated by Eq. (3).

2.4 Share of axial compressive force by surrounding concrete outside confining range of spirals

We imagine the force flow of concrete when spirals are reinforced under anchorage plate. Although we can explain inclined cracks and force flow due to the concentrated force of spirals, we cannot get enough test data for a quantitative strength evaluation. Thus we use shear friction test results for the analysis.

The shear friction strength formula developed by Nielsen,[4] which is based on the Hofeck's shear friction test data[15] is shown as follows.

$$\frac{\tau}{f'_c} = \gamma \cdot \frac{1 - \sin\phi}{2} + \phi\tan\phi \quad (7)$$

Where,

τ = shear strength

γ = ratio of concrete plastic strength to uni-axial strength, which is called the effectiveness factor

ϕ = friction angle according to the Coulomb failure criteria

φ = angle between loading and reinforcement direction

For normal concrete, we can substitute $\gamma = 2/3$, $\phi = 37^\circ$, then the equation without reinforcement is reduced to;

$$\tau = 0.113f'_c \quad (8)$$

In this study, we assume that a shear friction failure occurs when the shear stress of core concrete at surface exceeds the estimated value from Eq. (8).

The friction coefficient of concrete placed monolithically as specified in ACI code can be regarded that inclined angle of compressive force is about 35°. Thus, the stress flow is to have an angle of inclination of 35° in this study.

Since we assume an anchorage zone is subject to a radial pressure transverse to the member axis as shown in Fig. 1(c), the strength is determined by surrounding concrete. If we assume circular cross section inscribed in member section, inclined cracks

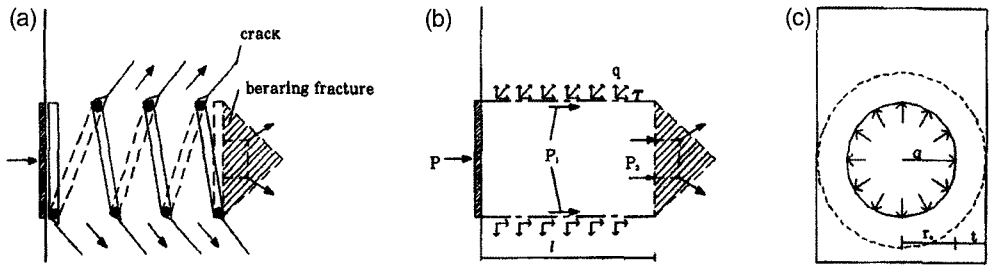

Fig. 1 Failure mechanism and model of the local zone outside the spiral (a) Failure mechanism of surrounding concrete, (b) Model of failure mechanism surrounding concrete, and (c) Sectional stress of shear friction failure mechanism.

develop at outer concrete while core concrete is not cracked.[16] According to the elasticity theory[17] we can calculate radial and circumferential stress at r under radial pressure.

$$\sigma_r = \frac{E_c}{1-\nu^2}\left[C_1(1+\nu) - C_2\frac{1-\nu}{r^2}\right] \tag{9a}$$

$$\sigma_\theta = \frac{E_c}{1-\nu^2}\left[C_1(1+\nu) - C_2\frac{1-\nu}{r^2}\right] \tag{9b}$$

Where,

$$C_1 = \frac{\sigma_1(1-\nu)}{E_c}\cdot\frac{\bar{r}^2}{\bar{r}^2-a^2}$$

$$C_2 = \frac{\sigma_1(1+\nu)}{E_c}\cdot\frac{a^2\cdot\bar{r}^2}{\bar{r}^2-a^2}$$

$$\sigma_1 = q\left[(1-\nu)\frac{\bar{r}^2}{b^2-\bar{r}^2} + (1+\nu)\frac{b^2}{b^2-\bar{r}^2}\right]\cdot\{(1-\nu)$$

$$\left[\frac{\bar{r}^2}{b^2-\bar{r}^2} + \frac{\bar{r}^2}{\bar{r}^2-a^2}\right] + (1+\nu)\left[\frac{b^2}{b^2-\bar{r}^2} + \frac{a^2}{\bar{r}^2-a^2}\right]$$

$$\sigma_2 = q\left[(1-\nu)\frac{\bar{r}^2}{\bar{r}^2-a^2} + (1+\nu)\frac{a^2}{\bar{r}^2-a^2}\right]\cdot\{(1-\nu)$$

$$\left[\frac{\bar{r}^2}{b^2-\bar{r}^2} + \frac{\bar{r}^2}{\bar{r}^2-a^2}\right] + (1+\nu)\left[\frac{b^2}{b^2-\bar{r}^2} + \frac{a^2}{\bar{r}^2-a^2}\right]\Bigg\}^{-1}$$

$$\bar{r} = \frac{b}{6}\cdot\frac{1+\left(\frac{a}{b}\right)+\left(\frac{a}{b}\right)^2}{1+\left(\frac{a}{b}\right)}$$

q = internal pressure
E_c = elastic modulus of concrete
ν = Poisson's ratio of concrete
Other signs are noted within Fig. 2.

Outer concrete is under biaxial stress state, *i. e.* radial compressive stress expressed by Eq. (9a) and circumferential tensile stress expressed by Eq. (9b). Compressive strength of the biaxial stress state depends on surrounding reinforcement out of the spiral, which can be determined by Eq. (1) in consideration of the strain on the reinforcements. Since circumferential tensile stress makes cracks when it exceeds a certain tensile strength, the surrounding

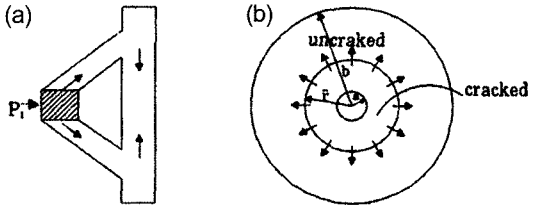

Fig. 2 Geometry of a disk loaded (cracked) by radial pressure (a) Side view and (b) Section view.

reinforcements must bear the tensile force after the crack. Thus the failure mode of surrounding concrete is either compressive failure of inclined compression strut of concrete or tensile yield of surrounding reinforcements.

Total force P is comprised of part P_1 shared by the surrounding concrete and part P_2 shared by the concrete ahead of spiral end. The ratio of P_1 to P_2 is the same as area ratio of each concrete.

$$P_1 = C_3 \cdot P \tag{10a}$$

$$P_2 = C_4 \cdot P \tag{10b}$$

Where $C_3 = 1 - \frac{A_{core}}{A_g}$

$$C_4 = \frac{A_{core}}{A_g}$$

A_{core}: Area of core concrete in spirals
A_g: Gross area

3. Construction of a mechanical model at the force-induced zone

3.1 Geometrical construction of the model

Marti[18] claims that there are three different kinds of models based on the plasticity theory. They are the STM with uni-axial strut and tie, fan-shaped stress field model and arch model. thürlimann reports that fan-shaped stress field model at force-induced zone shows the same stress resultants as the STM (Fig. 3a).

We can determine the location of meeting point of stress resultants by equilibrium condition and geometrical condition.

Equilibrium condition:

$$\sigma_0 \cdot b_0 \cdot t = \sigma \cdot b \cdot t \tag{11a}$$

$$\sigma_0 / b = b / b_0 = r / r_0 = h / h_0 \tag{11b}$$

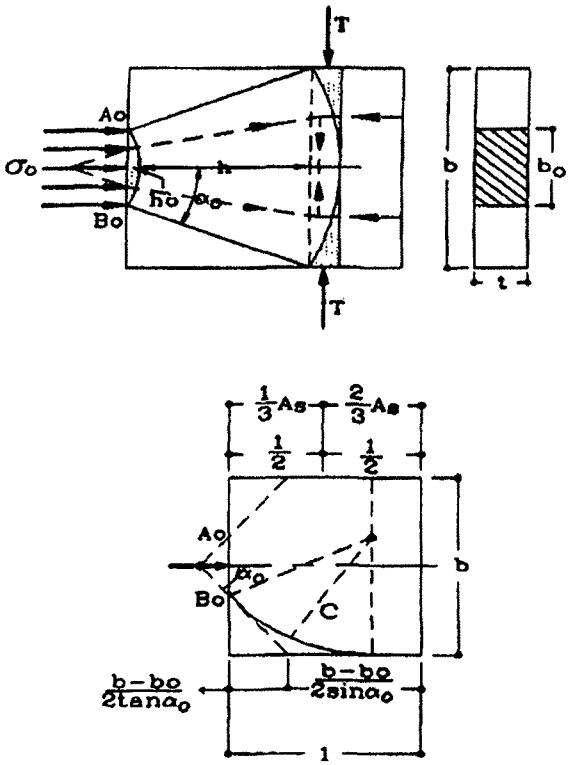

Fig. 3 Fan-shaped stress field.

Geometrical condition:

$$r_0 = \frac{b_0}{2\sin\alpha_0} h_0 = r_0(1-\cos\alpha_0) = \frac{b_0}{2}\frac{1-\cos\alpha}{\sin\alpha_0} \tag{12}$$

If we put $l \approx b$ according to Saint-Venant principle,

$$b = \frac{1}{2}(b-b_0)\cot\frac{\alpha_0}{2} \rightarrow \alpha_0 = 2\tan^{-1}\left\{\frac{1}{2}\left(1-\frac{b_0}{b}\right)\right\} \tag{13}$$

Transverse tension is shown as follows:

$$T = \alpha \cdot h \cdot t = \alpha \cdot b_0 \cdot t \cdot \frac{1}{2} \cdot \frac{1-\cos\alpha_0}{\sin\alpha_0} = \frac{P}{2} \cdot \tan\frac{\alpha_0}{2} \tag{14}$$

Then,

$$T = 0.25P\left(1-\frac{b_0}{b}\right) \tag{15}$$

This equation is the same as Mörsch's equation derived by simple truss model, which shows similar results from finite element analysis. Comparing with Guyon's results widely used by practical engineers, it generates conservative, larger values at the range of $b_0/b \geq 0.15$. If $b_0/b < 0.15$, we can use the above equation, since large local stresses calculated by elasticity theory does not happen in reality because of stress redistribution.

3.2 Geometrical construction of nodes

The points, nodes, where stress resultants change their vector direction, are found at the zone directly under anchorage plate and at the point where tie and compressive resultant meet. We call each node as C-C node and C-T node, of which position can be determined by general methodology of the STM. Although nodes are an imaginary concept, we can use the node location to build a simple mechanical model.

For the C-C nodes, stress wedge of 45° angle is assumed, and each P/2 force acts at $b_0/4$ point, which changes the direction at the stress wedge. C-T nodes are the points, where stress resultants from the stress wedge and stress resultants of transverse direction meet.

We can get an angle θ of the stress resultant to the member axis and the meeting point as follows.

$$\tan\theta = \frac{1}{2}\left(1-\frac{b_0}{b}\right) \tag{16}$$

$$y = \frac{b_0}{4} + \frac{1}{4}(b-b_0)\cot\theta \tag{17}$$

The width of the stress field is then calculated by geometrical constraint.

$$w_1 = \frac{b_0}{2}(\sin\theta + \cos\theta) \tag{18a}$$

$$w_2 = \frac{b}{2}\frac{1}{\cos\theta} \tag{18b}$$

When the member is reinforced by the spiral, P is shared by P_1 and P_2 as shown in Eq. (10), which are the resultant forces working at outer and inner side of the spiral. In the zone outside the spiral, the force spreads at an angle of θ_1 from a half the length of the spiral confining zone and meets with transverse tensile force. At the end of the spiral, P_1 force acts, of which the bearing area is the same as that of core. Now, the geometrical location of nodes can be determined by Eqs. (16) and (17). As shown in Fig. 7, y_1 and y_2 values determine the nodal point.

$$y_1 = \frac{1}{2}l_s + \frac{b}{4}\cos\theta_1 \tag{19a}$$

$$y_2 = l_s + \frac{d_s}{4} + \frac{1}{4}(b-d_s)\cos\theta_2 \tag{19b}$$

Where, l_s = the length reinforced by spiral,
d_s = diameter of core concrete,
$\theta_1 = 35.5°$ when the friction coefficient is 1.4, and
θ_2 = determined from Eq. (16).

3.3 Strength of the model

Since the mechanical model is constructed by an equilibrium equation, the strength of each element determines the strength of the whole model.

Failure modes and the element strength being considered are given as follows;

- bearing failure of C-C node: bearing strength by Eq. (3),
- compressive failure of inclined compressive strut: bi-axial compressive strength by Eq. (1), where principal tensile strain is given by Eq. (2) when transversely reinforced,
- tensile failure of tensile reinforcements: yield stress of reinforcements, where we consider the reinforcements centered by tension resultants,
- shear friction failure between core concrete surrounded by a spiral and surrounding concrete outside the spiral: shear friction strength by Eq. (8),

- tensile failure of reinforcements at surrounding concrete outside the spiral: tensile strength of reinforcements, assuming tensile stress by Eq. (9) acts on the total length of spiral confining zone,
- bearing failure of the concrete wedge of spiral end: bearing strength by Eq. (3),
- compressive failure of core concrete: compressive strength by Eq. (6).

4. Application examples and review

The proposed mechanical model is applied to several typical test members, and the results are compared with experimental results and other study. Selected examples are rectangular members of a well-known test series.

4.1 Example1: rectangular section not reinforced by spiral

We select test member A3 of Sander's test series, which has the properties shown in Table 1 and is reinforced as shown in Fig. 4.

4.1.1 Construction of a model

A mechanical model constructed by the principles discussed in section 3 is shown in Fig. 5. The strength of each element is calculated, and the failure modes and the maximum strength are shown in Table 2. In building the model, we assume the strut width as an average value of w_1 of C-C node and w_2 of C-T node. Furthermore, we assume the strain of reinforcements is ε_y.

Table 1. Material properties of test specimen A3.

Property	Value
Concrete strength	23.9 MPa
Steel yield stress	555.0 MPa
Steel Young's modulus	2.04×10^5 MPa

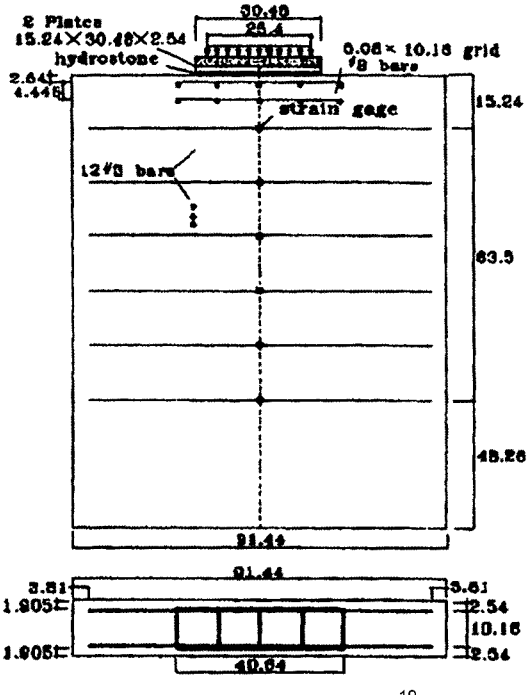

Fig. 4 Test specimen A3.[19]

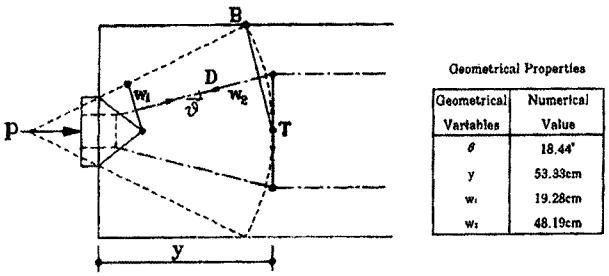

Fig. 5 Construction of the model.

Table 2. Strength of each failure mode.

(unit : kN)

Failure mode	Strength of the members	Calculated max. load
Stirrup yield	474.8	284.8
Bearing failure under plate	943.7	943.7
Inclined compression strut failure	914.3	1735

4.1.2 Comparison with test result and other study

At 1109 kN and 1177 kN, the first crack and failure, respectively, were observed. The failure mode was bearing failure type, where stirrups remained elastic until failure.

Comparing the test values against the results reported in other study (by Sanders) by nonlinear finite element analysis and the proposed model. For the nonlinear finite element analysis, DIANA program was used, and the yield criteria and tension stiffening model are shown in Table 4. The values calculated by the proposed model were lower than those computed by the nonlinear analysis but more consistent and realistic than the other two models. The main difference from the other two models was not the failure load but the failure mode. The other two STMs expects a 'node-structure interface failure', while the proposed model expects 'bearing fracture failure' mode. Reports shows that concrete under the anchorage plate fractures and does not yield lines as expected by plasticity theory. Since 'Node-structure interface' of STM is an idealistic model, the estimation of the strength is not so accurate. In addition, the failure mode is not clearly distinguished from the bearing failure mode at C-C node. For the sake of this analysis, the 'bearing failure' is assumed to include the 'non-structure interface failure.'

4.2 Example 2: rectangular section reinforced by a spiral

We select the test member, Beam 1 of Woolman's test series,[20] which is reinforced as in Fig. 6 and has properties shown in Table 2. The test member is similar to Sander's test member B3, previously discussed, while it is described in more detail.

4.2.1 Construction of a model

A mechanical model constructed by the principles previously discussed in this section 4 is shown in Fig. 7. The strength of each member is calculated, the failure mode and maximum strength are shown in Table 6. In constructing the model, we assumed effective reinforcements lie in the zone of length $2y_1$, where y_1 is the location of tensile stress resultant. Proportional shares of the force P, P_1 and P_2, are determined by the ratio of core and surrounding concrete.

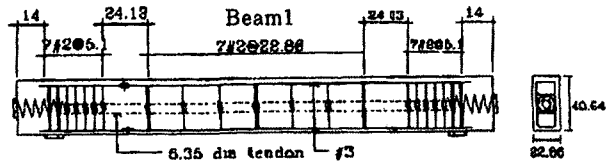

Fig. 6 Test specimen beam 1.[20]

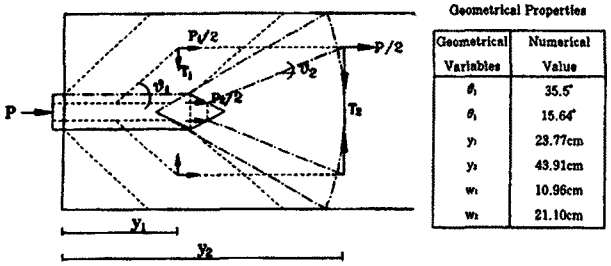

Fig. 7 Construction of the model.

Table 3. Comparison of various calculations and test result.

Model	Predicted (or test) load	Failure mode	P_{test} / P_{cal}
Test, ultimate (experimental value)	1,177	Bearing fracture	–
Conventional STM[16]	907.4	Node-structure interface failure	1.30
Modified STM[16]	889.8	"	1.32
Proposed model	943.7	Bearing fracture	1.25
Nonlinear finite element	1,059	Bearing fracture	1.11

Table 5. Material properties of test specimen beam1.

Property	Value
Concrete strength	36.4 MPa
Steel yield stress	448.5 MPa

Table 6. Strength of each failure mode.

Failure	Strength of the members	Calculated max. load
· Stirrup yield (by Tension T2)	197.6	2297
· Inclined compression strut fracture	1213	2779
· Core in spiral fracture	1712	1712
· Shear friction of spiral by confining stirrup yield*	1172	2464
· Bearing failure at the end of spiral*	1146	2017
· Shear friction failure between spiral and surrounding concrete*	643.6	1490

(unit : kN)

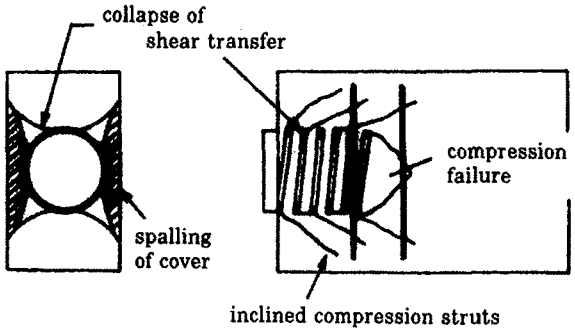

Fig. 8 Failure of concrete surrounding the confined core.

Tensile failure mode by a radial tension at surrounding concrete is governed by yielding of the reinforcements. Since the failure strength of the strut was very large, the result was treated as an unexplainable outlier. The three failure modes in the Table occurred consequently, i.e. if one of those failure modes took place, then the other elements was burdened by the previous load.

4.2.2 Comparison with the experimental result

At 1,112 kN and 1,403 kN, the first crack and failure, respectively, were observed. At failure, surrounding concrete fell off and concrete at the end of the spiral fractured. Fig. 8 shows the failure amode.

As in example 1, most reinforcements stayed at low stress level up to the final failure, while the reinforcement surrounding a spiral yielded. This failure mode is a shear friction failure as predicted. Since shear friction failure and end zone concrete failure occurred consecutively, the final failure looked like a concurrent failure.

4.2.3 Comparison with other reported study

We compare the experimental values with the results reported in other study by Woolman, computed by nonlinear finite element analysis, and predicted by the proposed model in Table 7. For the nonlinear finite element analysis, we use values of Table 4, not considering the effect of the spiral. The results calculated by the proposed model were very similar to the experimental results of Woolman's result. The main difference from other STMs is the failure mode. Other STMs predict yield failure of reinforcement, while proposed model predicts shear friction failure as the critical

Table 4. Yield criteria for the nonlinear FEM analysis.

Concrete fracture criteria	Yield criteria	Mohr-coulomb, friction angle $\phi_0 = 37^o$
	Stress cut-off	Linear
	Tensile strength	$\sigma_t = 0.33\lambda\sqrt{\sigma'_c}(\mathrm{MPa})$, where $\lambda = 1.0$
	Shear retension	Constant shear retension, shear retention factor $\beta = 0.5$
	Nonlinear tension softening	Smeared crack model parabolic tension softening model
Steel yield condition	Yield criteria	Von mises yield criteria

Table 7. Comparison of various calculations and test result.

Model	Predicted (or test) load	Failure mode	P_{test} / P_{cal}
Test, ultimate (experimental value)	1403	Concrete surrounding spirals and ties spalled off, concrete ahead of the spiral was crushed	–
Conventional STM[19]	1481	Brusting tie yields	0.95
Modified STM[19]	1432	"	0.98
Proposed model	1491	Shear Friction failure between concretes *in and surrounding* the spiral, and bearing failure ahead of spiral follows	0.94
Nonlinear finite element	1148	Bearing fracture	1.22

failure mode. The computational result of nonlinear finite element analysis was significantly different from the experimental result. We construe that the main cause of the difference is of the dimension of the modeling. Two-dimensional analysis by nonlinear finite element method cannot give a good prediction for three-dimensional failure mode like this member, although it tends to result in a good prediction for two-dimensional failure like the previous example.

5. Conclusion

In this study, we constructed a mechanical model for the end anchorage zone of prestressed concrete members based on the plasticity theory and concrete material properties. The following conclusions from comparison study of the proposed model and typical test results the are presented.

1) The proposed mechanical model showed a similar or better estimation of the failure load than other analysis models.

2) The proposed model showed some advantages in predicting the failure mode. Using this advantage, we could better predict a shear friction failure between core and surrounding concrete and we found that a bearing failure at the end zone of core concrete occurred successively after the shear friction failure.

3) Two-dimensional finite element analysis is effective for two-dimensional failure analysis, while it shows some shortcomings in its application to three-dimensional failure mode, which occurs at the anchorage zone reinforced by a spiral.

4) From this study, it can be safely concluded that the proposed mechanical model explained the mechanical behavior of the concrete members and partly overcame the limitation of two-dimensional analysis, even though it was not meant to replace the most accurate experimental methods or other more refined analysis.

Acknowledgements

This study has been funded by Dong-A university. The authors hereby express sincere appreciation for the support.

References

1. Schlaich. J., Schäfer, K., and Jennewein, M., "Towards a Consistent Design of Structural Concrete," *PCI Journal*, Vol.32, No.3, May-June 1987, pp.74~151.

2. Guyon, Y., *Prestressed Concrete*, John Wiley and Sons, New York, 1953.

3. Leonhardt, F. and Mönnig E., *Vorlesungen ber Massivbau*, dritter Teil, Grundlagen zum Bewehren in Stahlbetonbau, Springer-Verlag, 1977.

4. Nielsen, M. P., *Limit Analysis and Concrete Plasticity*, The University of Denmark, 1984.

5. Thürlimann, B., Marti, P., Pralong, J., Ritz, P., and Zimmerli B, *Anwendung der Plastizitätstheorie auf Stahlbeton*, Institut für Baustatik und Konstruktion, ETH Zürich, Autographie zum Fortbildumgskurs für Bauingenieure aus der Praxis, April, 1983.

6. Schlaich, J. and Weischede, D., "*Zum methodischen Bemessen und Konstruieren*," DAfstb Heft 150, 1982.

7. Schlaich, J. and Schäfer, K., "*The Design of Structural Concrete*," The University of Stuttgart, IABSE workshop New Delhi, 1993.

8. Ahamd, S. H. and Shah, S. P., "Stress-Strain Curves of Concrete Confined by Spiral Reinforcement," *ACI Journal, Nov-Dec.*, 1982, pp.484~490.

9. Vecchio, F. J. and Collins, M. P., "Compression Response of Cracked Reinforced Concrete," *ASCE Journal of Structural Engineering*, Vol.119, NO.12, Dec., 1993, pp.3590~3610.

10. Muttoni, A., "*Die Anwendbarkeit der Plastizitätstheorie in der Bemessung von Stahlbeton*," Institut für Baustatik und Konstruktion ETH Zürich, Juni, 1990.

11. Collins, M. P. and Mitchell, D., "*Prestressed Concrete Structures*," Prentice Hall, Englewood Cliffs, New Jersey, 1990.

12. Hawkins, N. M., "The Bearing Strength of Concrete for Strip Loadings," *Magazine of Concrete Research*, Vol.22, No.71, June 1970, pp.87~98.

13. Kanellopoulos, A., *Zum unelastischen Verhalten und Bruch von Stahlbeton*, Institut für Baustatik und Konstruktion, ETH Zürich, Bericht Nr.153, 1986, 86pp.

14. Richart, F. E., Brandtzaeg, A., and Brown, R. L., *The Failure of Plain and Spirally Reinforced Concrete in Compression*, University of Illinois, Engineering Experiment Station, Bulletin 190, April 1920, 71pp.

15. Hofbeck, J. A., Ibrahim I. O. and Mattock A. H., "Shear Transfer in Reinforced Concrete," *J. ACI., Proc.*, Vol.66, Feb. 1969, pp.119~128.

16. Yankelevsky, D. Z., "Bond Action Between Concrete and a Deformed Bar-A New Model," *ACI Journal*, Vol.82, No.2, March-April, 1985, pp.154~161.

17. Sokolnikoff, I. S., *Mathematical Theory of Elasticity*, 2nd Edition, McGraw-Hill Book Co. New York, 1956, 476pp.

18. Marti, P., "Basic Tools of Reinforced Concrete Beam Design," *ACI Journal*, Vol.82, No.1, January-February, 1985, pp.46~56.

19. Sanders, D. H., "*Design and Behavior of Anchorage Zones in Post-Tensioned Concrete Members*," Ph. D. Dissertation, The University of Texas at Austin, August 1990.

20. Wollmann, G. P., *Anchorage Zones in Post-tensioned Concrete Structures*, Ph. D. Dissertation, University of Texas at Austin, 1992, pp.62~98.